CERN/MPS/CO 69-14
26 June, 1969

A SERVO CONTROLLED TARGET MECHANISM FOR THE CERN PS

J.J. Merminod, M. van Rooy

* * *

A SERVO-CONTROLLED TARGET MECHANISM FOR THE CERN PS

1. Introduction

1.1 What is an internal target mechanism?

Internal targets are mainly used to convert the circulating proton beam into other particles which are then used in the experimental areas[1].

Sometimes targets are used for other purposes, such as beam measurements[2] or to deviate protons which would otherwise hit a septum[3]. In all these cases, the working position is somewhere in the middle of the vacuum chamber. This we call "up" position. At injection the full aperture is needed for the proton beam. Then the target should be located somewhere outside this aperture. This may be above the vacuum chamber, but it is always called the "down" position. This calls for a mechanism which gives the target the necessary displacement: a target mechanism. Mostly two target mechanisms are grouped together inside a vacuum cover with a standard square flange; this is then a target unit. The square flange fits the standard target position which are the box-like enlargements of the vacuum chamber between the coils at the downstream end of each magnet. They have a hole of ∅ 120 mm on the inside and on the outside, normally covered with a similar square flange.

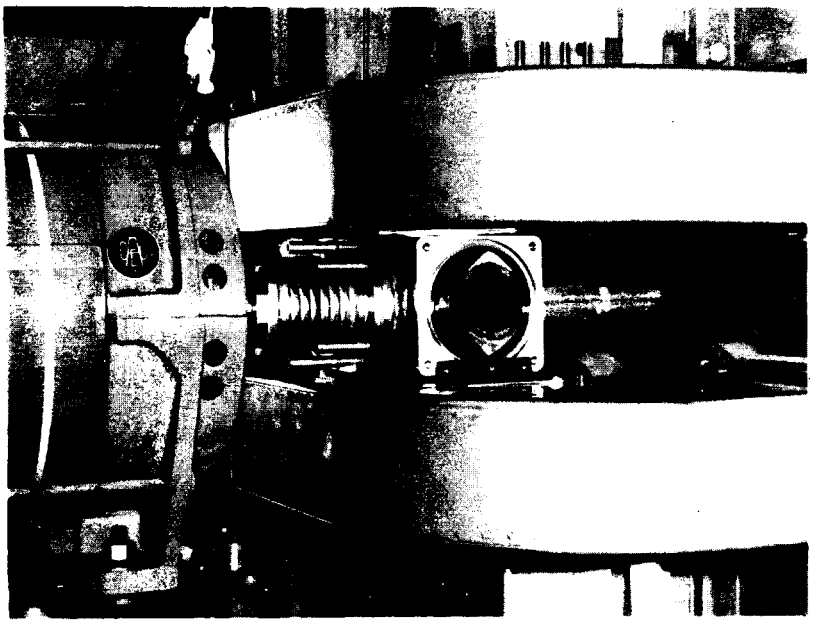

Photo 1

A standard target position

1.2 Requirements

This target mechanism has to satisfy several demands:

a) the mechanism is completely remote-controlled;

b) the movement between "down" and "up" positions and return should be adapted to the machine cycle;

c) the "up" position should be reproduced at each cycle with a precision better than 0.1 mm;

d) the "up" position is adjustable in radial direction about 120 mm around the middle of the chamber and vertically about 10 mm around the same middle. Both adjustments measured and reproduced with an accuracy of $\pm$ 0.1 mm;

e) the mechanism has to be able to handle the different sizes and shapes of targets used, up to 20 gr. weight, with simple adjustments.

Besides these specific requirements there are, of course, the general PS equipment rules like vacuum suitable, no disturbance of the machine magnetic field, insensitive to external magnetic fields and, since it becomes fairly radio-active[4] during use, easy to handle and to maintain. For the same reason the materials used for the mechanism should all have a good resistance against radiation. This applies specially to any insulating materials[5].

1.3 Why a new type?

Since the start of the operation of the CPS, internal targets have been in use and their mechanisms are described in various reports[6].

However, when in 1965 the CPS Improvement Programme[7] started, an increased repetition rate was also planned and this, together with more complex sharing operations, would put a heavy load on the existing target systems. Especially the rise-time and its stability needed improvement in order to be able to put closely together different operations during one machine cycle without the risk of them overlapping now and then.

This fixed the rise time at about 30 msec, as opposed to about 100 msec for the existing type, but even more important was a very small jitter, that is difference in rise time from pulse to pulse.

1.4 The first steps

Around September 1964, the Targets Section of the MPS Controls Group started on this new project. In any case, the new mechanism should fit inside the already existing target chassis (Photo 2), which would give

Photo 2

it the necessary radial displacement and which would provide the vacuum cover with the standard flange. This fixed, of course, many maximum dimensions.

Two different approaches were made.

A. An arm, about 400 mm long bears on one end the target and the other end is attached to a set of crossed springs which allows it to swing around an angle of 5° and which gives it at the same time a free swinging frequency of about 20 cycles/second, depending on the weight of the target. The low inertia motor, already in use for the target system '63, drives this arm with a directly-coupled swivelling axle,

located at the point where the springs cross. Both end positions are secured by this axle being at one of its dead points, and the speed with which the arm swings from one to the other is almost entirely defined by the acceleration the crossed springs give to it.

The power supply for this mechanism is almost the same as the existing one for system 63[8]. The only difference is an extra device able to give alternating pulses to the motor to get the arm from its normal rest position somewhere in the middle of the stroke, to one of the end positions (Photo 3).

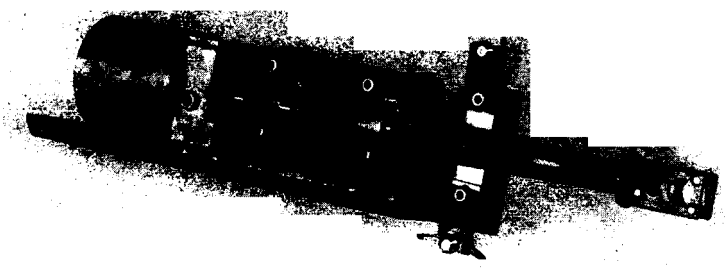

Photo 3

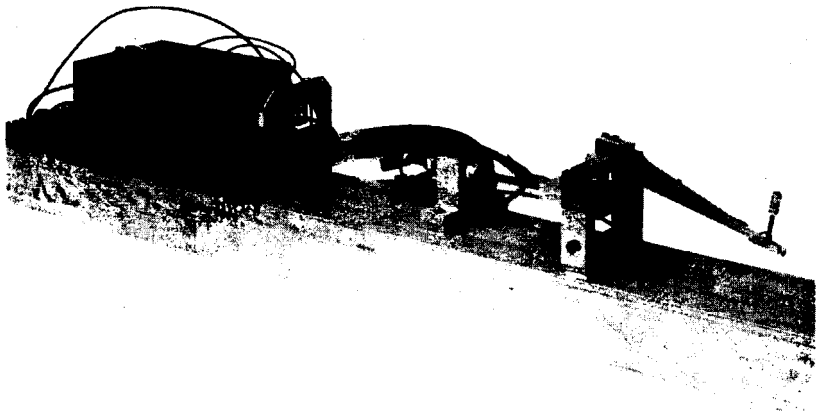

Photo 4

B. An arm, about 150 mm long, holds the target on one end and the other end has knife-edge suspension. A coil is suspended on this arm via a spring at a distance of about 22 mm from the rotation point on the knife edges and on a spider. It sits in the gap of a strong electro magnet and when a current passes a force is exerted on it and it pushes the arm around an angle of $\sim 15^{\circ}$ for a stroke of 6 mm. Its position is continuously measured with a linear differential transformer of which the metal core is fixed to the coil (Photo 4). With these components the power supply can impose on this motor a certain time displacement function with the feedback of the signal of the transformer, a servo system.

After the first tests in the lab of the two systems, it was decided to build an operational prototype of the servo target mechanism, in order to investigate its functioning under real machine conditions. Early in 1966 the design work started and towards the end of the year the parts were manufactured. After several improvements mainly concerning stiffness of force transmitting parts and the coil, it was tested in the CPS during weeks 9 and 10 in 1967.

The results of this test led to the decision to build a batch of eight of these target mechanisms. While waiting for tenders from manufacturers to arrive, a few more lab tests were made. A lifetime test, extended to 14×10^{6} cycles, with repetition rates up to 8 per second, was executed, measuring at the same time the temperature rise of the coil when working in a vacuum of 5×10^{-6} Torr. The change in resistance of the coil was measured to find this temperature rise and for 8 cycles per second it was found to be 50° C. For the expected maximum repetition rate of 1 cycle per second, with the target staying "up" for 100 msec, the temperature rise was about 15° C after 24 hours' running.

2. Design of the system

2.1 Electronic design

2.1.1 Principle

The aim was to let the target make its stroke of 40 mm in 25 msec. The curve time - displacement E, which gives for a certain permissible

acceleration the wanted stroke in minimum time, is shown in Fig. 5, together with the corresponding curves for the speed V and for the acceleration γ, for this movement of uniform and equal acceleration and retardation. The acceleration $\gamma = 2\frac{E}{t^2}$ where E is half the total stroke and t is half the total time, which gives $\gamma = 256\ msec^{-2}$, which is about 26 g.

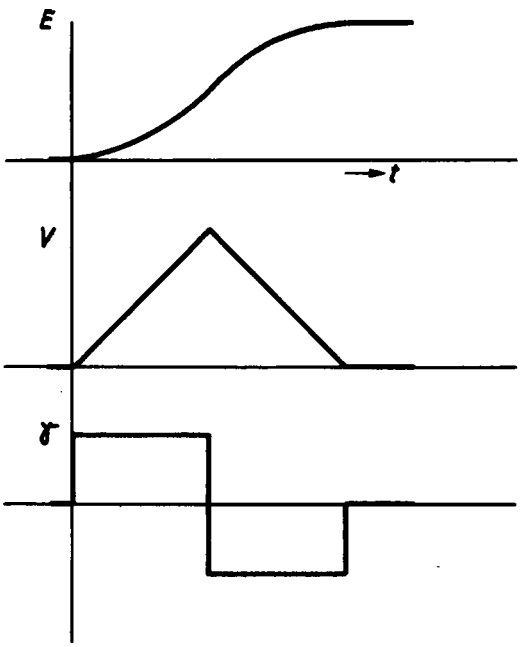

Fig. 5

This movement is obtained with a position servo loop shown in Fig. 6 below. It is a linear DC servo system with the exception of the position captor which is a linear differential transformer without friction and radiation resistant. It receives a 2 kc input signal from an amplitude stabilized oscillator. The timing and control circuits as well as the function generator are installed in the Main Control Room. They generate a programmed tension which is sent down to the power servo-circuit in the PS ring, installed close to the target but shielded from its radiations. From there a 25 metre multicore cable goes to the target unit.

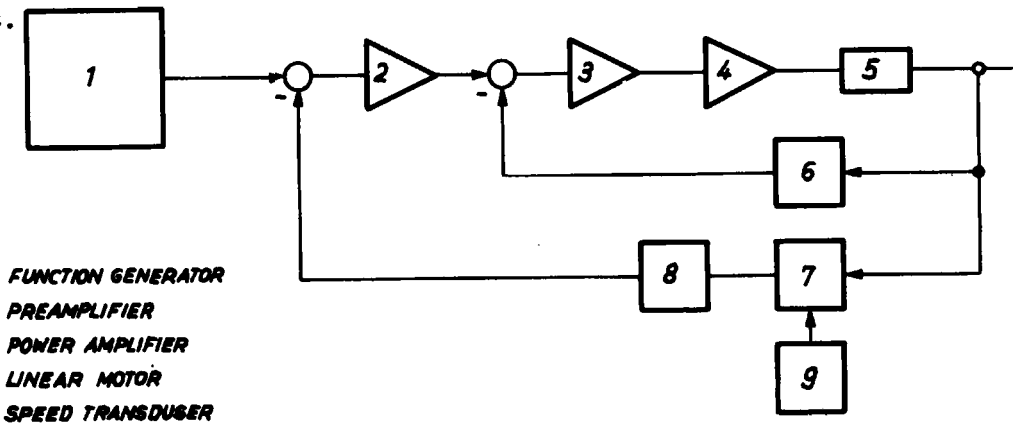

1 FUNCTION GENERATOR
2,3 PREAMPLIFIER
4 POWER AMPLIFIER
5 LINEAR MOTOR
6 SPEED TRANSDUCER
7 DIFFERENTIAL TRANSFORMER
8 DEMODULATOR
9 OSCILLATOR

Fig. 6

2.1.2 Description of the circuits

a) The function time-tension, generated in the MCR, and which the target has to follow as a function time-displacement, is represented in Fig. 7. The maximum amplitude is 20 volts, corresponding to a stroke of 40 mm for the target. The "down" position is fixed and the "up" position can be varied by changing the stroke between 30 and 40 mm. The time Tp (up-time) is adjustable between 0 and 400 msec and the rise and fall times Tr and Tf are equal and adjustable between 5 and 100 msec, depending upon the weight and strength (fragility) of the target in use.

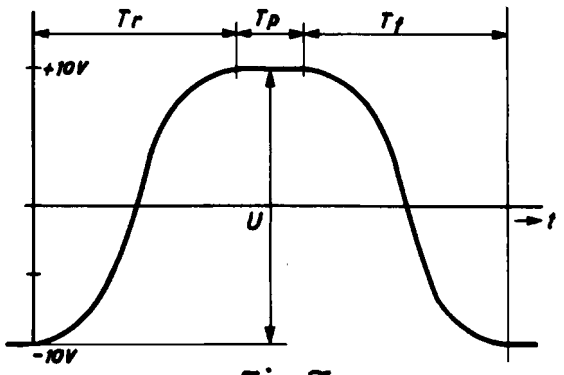

Fig.7

For the current operation with the actual heads, the setting is Rr = Tf = 25 msec.

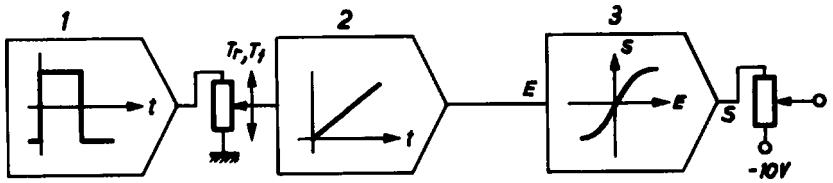

1 SQUARE WAVE GENERATOR
2 INTEGRATOR
3 FUNCTION GENERATOR

Fig.8

Fig. 8 above shows the block diagram of the function generator. A squarewave function, after being attenuated by a potentiometer to adjust Tr and Tf, is integrated, giving a trapezoidal function. This feeds a function generator with diodes, which realizes the sinusoïdal function by approximation with 19 straight bits. At last a potentiometer with one end at -10 volts permits adjusting the amplitude

of the function without changing its starting value, which corresponds to the rest position of the target.

b) We have seen that the target is subject to high acceleration under actual conditions. At the same time, these targets are very fragile since one wants to have them supported by as small a mass as possible in order to have a real point source for the secondary particles. A very much employed shape is an elbow, both parts having about 20 mm length and a round cross-section with about 1 mm diameter, made of beryllium. We expect to be using soon even smaller dimensions and more brittle materials (Al_2O_3 and BeO). From this, it is clear that a certain acceleration should never be exceeded due to the risk of breaking the target. This condition is fulfilled when the movement of the target follows the ideal generated curve. Particularly sudden changes in direction, caused by spurious trigger pulses for instance during movement of the target, are to be prevented. The switch-over from one target to the other should also be made without shock and should only be possible when both targets are at rest in their "down" position.

Faulty operations inducing the above errors in operation should be excluded by the electronic circuit layout. A device, simply limiting acceleration, is not sufficient for it would not exclude the hitting of the mechanical end stops, one placed just after the electrical "down" position and the other limiting the stroke to 45 mm.

The two main features of the solution chosen are

a) the simplicity of the control panel

b) the interlocking between different controls to prevent wrong operation.

Photo 9 shows the MCR crate with three drives, each one consisting of three plug-in units which are shown in photo 10.

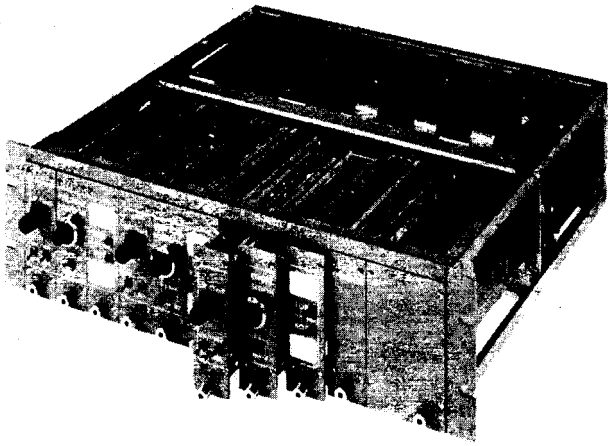

Photo 9

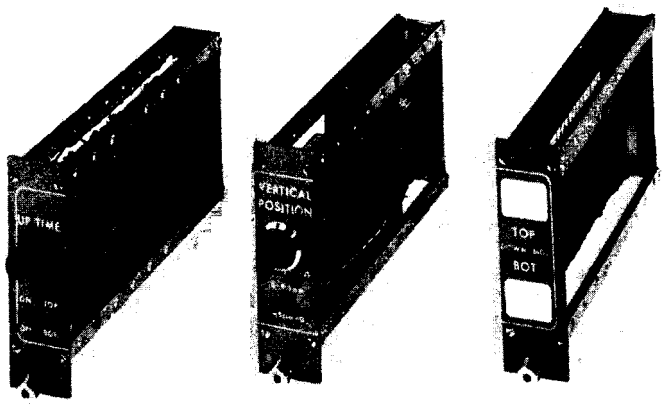

Photo 10

Diagram 11 shows a simplified form of the control circuit. The different interconnections and interlocks can be distinguished, necessary for security. In particular, the selector switch Top-Bot, which is inactive when the on-off switch is on. On the other hand the trigger input gate is closed when a commutation takes place.

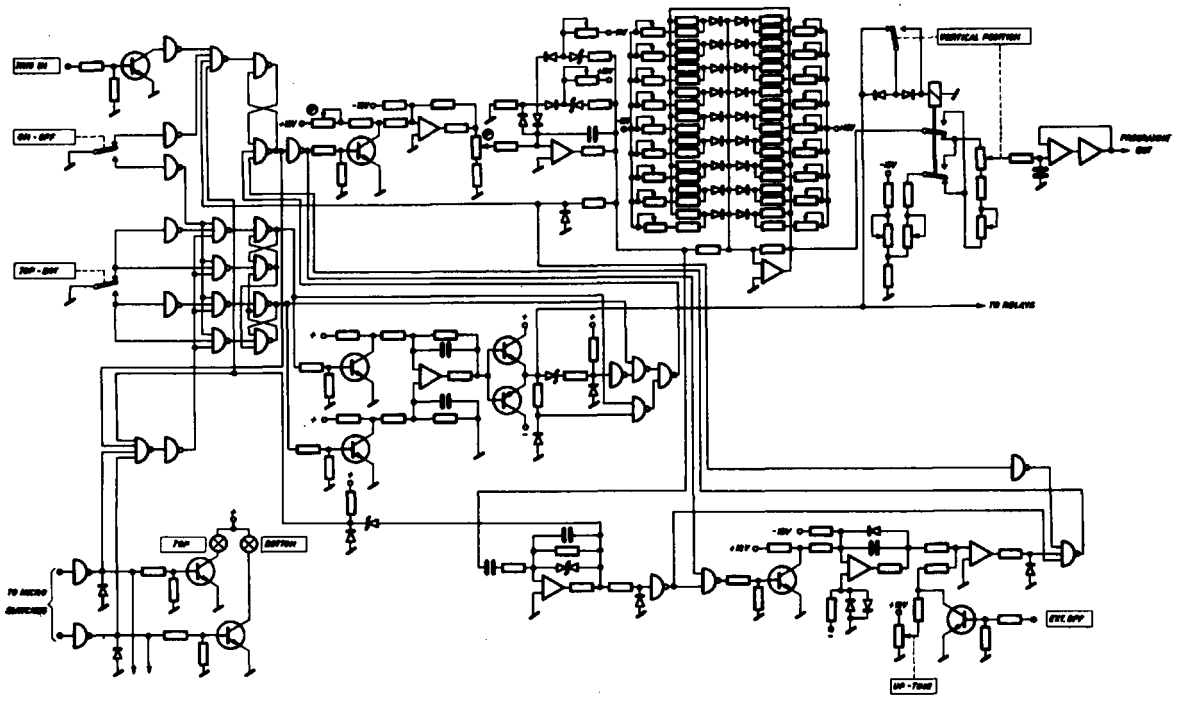

SERVO-ACTUATED TARGET
CONTROL CIRCUIT

Diagram 11

The control tension for the relays changes linearly during the first 100 msec. This allows a selective control in time for the commutating relays by appropriate choice of attracting and falling-off tensions. In this way the disconnecting as well as the switch-over Top-Bot is always done in the right sequence.

c) The Ring chassis.

Photo 12 shows this chassis and diagram 13 the principle, with only one target motor for simplification.

The function time - voltage, generated in the Main Control Room is received by a differential amplifier which assures the common mode rejection. The 2 kc oscillator which feeds the linear-differential transformer is stabilized in amplitude with a servo loop which uses a thermistor with indirect heating as a control device. The power

amplifier has the bridge configuration which gives an output voltage almost twice as high as the power transistors themselves.

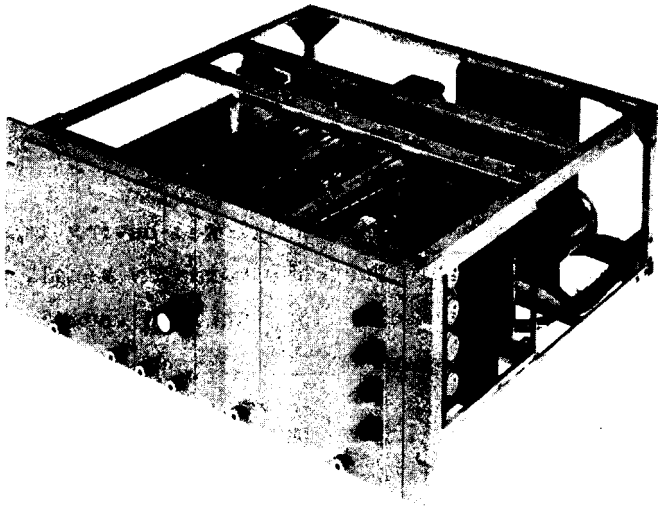

Photo 12

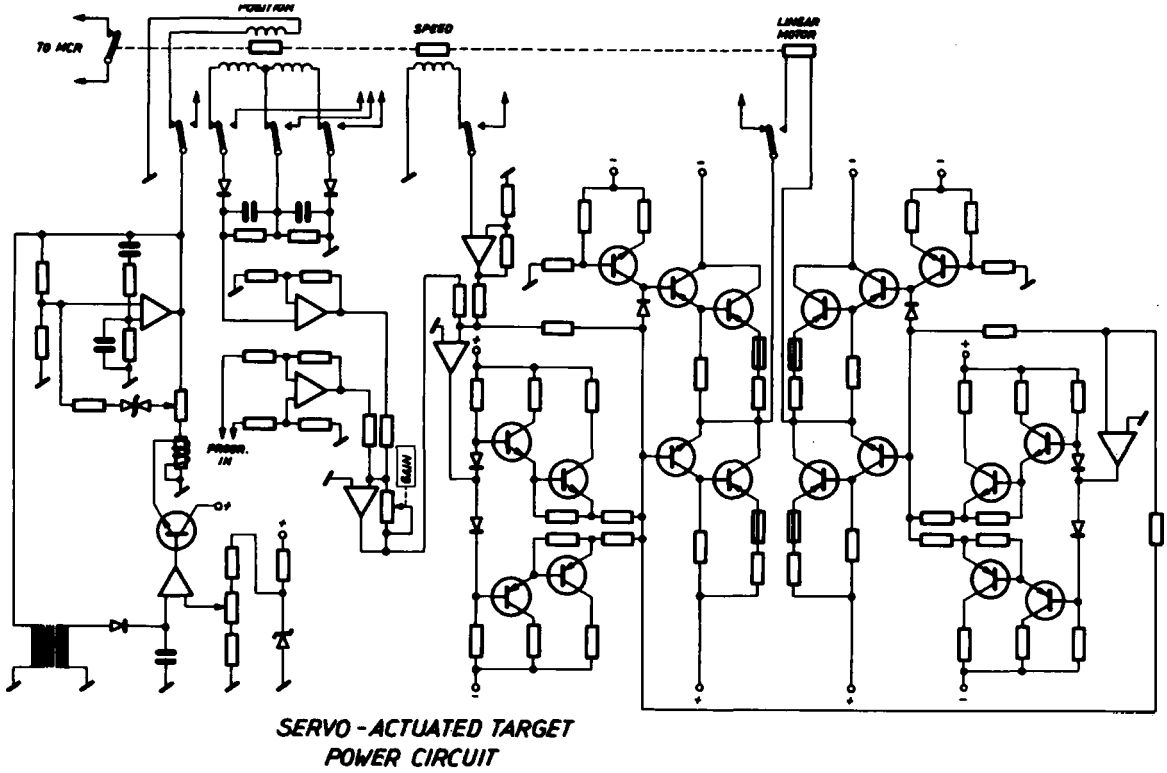

SERVO-ACTUATED TARGET
POWER CIRCUIT

Diagram 13

2.2 Mechanical design

2.2.1 Principle

Since the mechanism has to work in vacuum where adequate lubrication is excluded, it was tried not to have any friction in the system. This led to the solution to have all moving parts suspended on springs.

Up to now, most target mechanisms allowed having two targets in one standard target position. They are normally equal, one being the spare of the other, but separately adjustable in radial and vertical positions.

However, the servo motor is too bulky to have two of them moving independently inside the existing radial unit chassis (Photo 2) and it was decided to have only one chariot, radially adjustable, consisting of two independent motors, one moving a target from above the aperture down to the working position, the other moving a target from below up to the middle of the chamber. The two targets cannot be "up" at the same time.

This simplifies in so far as the power supply is concerned in that there is only one per target unit, with a switch to select "top" or "bottom", which controls relays in the power servo circuit in the PS ring close to the target. From the point of view of space in the MCR, three units high in a 19" rack now control three target units while the system '63 needs four units high to control two target units.

In the double target mechanism, each motor has three components :

a) a coil, moving in a magnetic field,

b) a speed captor,

c) a position captor.

The arm which moves the target and the motor connecting rod, which links the motor components, have together one set of springs which assures the guidance of all. Instead of the round coil a flat one is used for space requirements and this gives a system which looks roughly

like Fig. 14 where the springs are only indicated by the turning points they create.

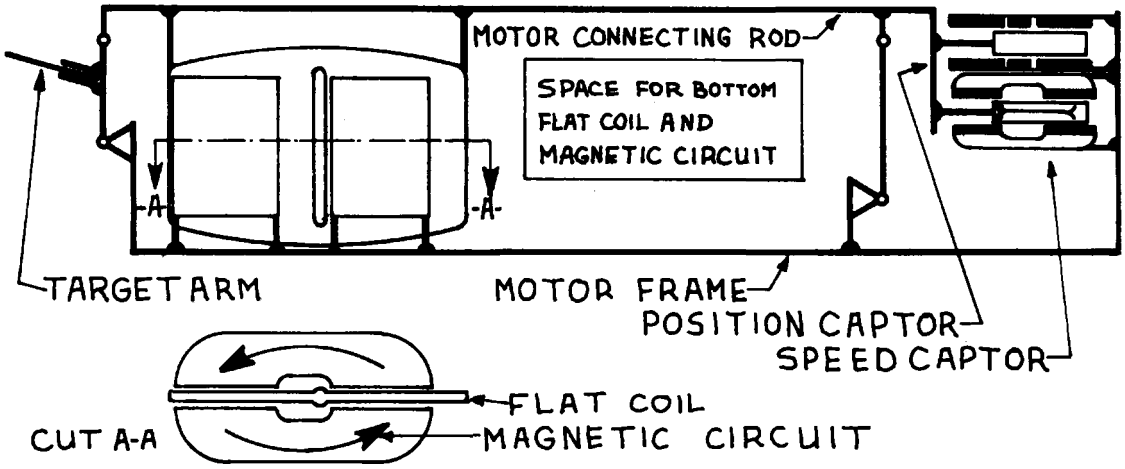

Fig. 14 Lay-out of servomotor.

Photo 15 shows the actual mechanisms without the target arms.

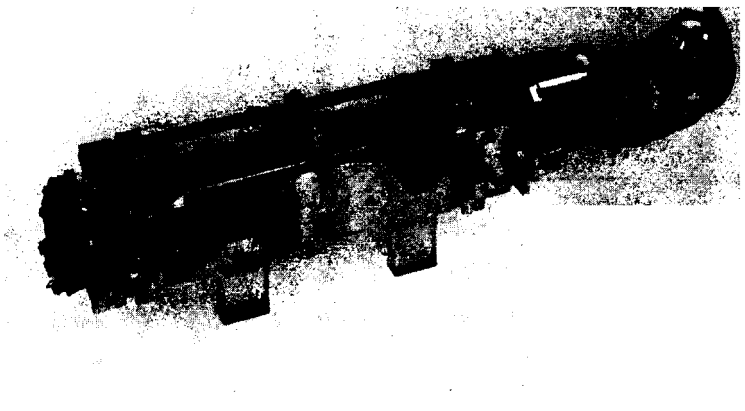

Photo 15

Photo 16 shows the mechanism inside the radial unit chassis and photo 17 shows target unit 37 ready to be mounted in ss 01.

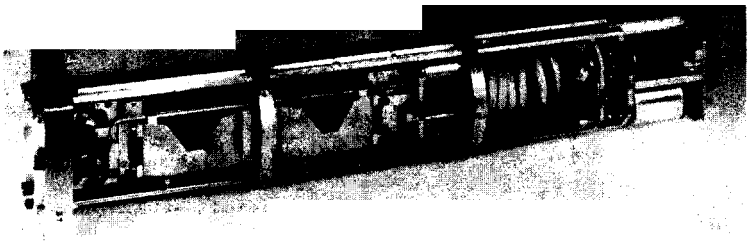

Photo 16

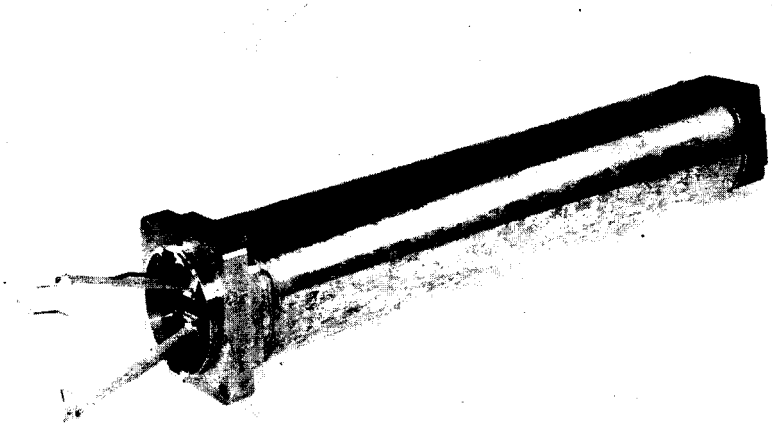

Photo 17

2.2.2 A few components

a) The flat coil

The first trial was to make it as a printed circuit on a steatite base. This proved very inefficient since the base represented too large a part of the weight and volume.

Then the coil was wound between two flanges with thermofix D wire. When the required number of turns (~ 90) was reached, a strong

current was passed through it which baked together the turns and then the coil could be dismounted without uncoiling. The next step was to put this coil in an appropriate mould and cast it under vacuum in filled polyester resin which gives it its final shape and strength (Photo 18). The wire used has a copper diameter of 0.65 mm giving a resistance of ~ 1.4 ohm to the coil. The impedance is kept low in order to get a good time response.

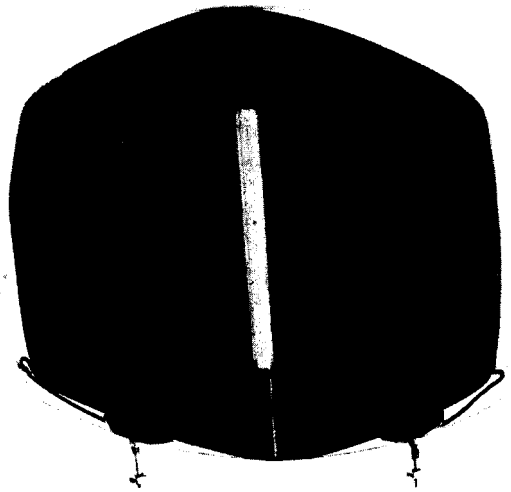

Photo 18

b) A reed switch, operated by a small permanent magnet, indicates when the target is in its "down" position.

c) The motor connecting rod links all the componenents together and transmits the pushing force from the motor to the arm which carries the target. Its importance was initially overlooked which caused a lot of trouble. The reason was that the force of the flat coil, which is about 6 kgs maximum, bent this beam and this moved the captors in a direction opposite to the one which would follow from the direction of the current in the coil. This upset of course the servo system and started vibrations, which the suspension of the whole system on springs did not help very much to suppress. An electronic circuit added to each motor adjusts for each the attenuation of the feedback signals above a certain frequency. This, together with the redesigning of the motor connecting rod, making it as strong as possible in the available space, limited these vibrations to an acceptable value.

d) The springs are all made of copper beryllium for its excellent qualities as regards fatigue, stress and non-magnetism. They are arranged in such a way that the target is kept in its "down" position when the motor is free from current. Some of these springs have to transmit high forces, whilst needing at the same time good flexibility to allow the arm to pivot around an angle of 13°.

Photo 19 shows the springs at the front end of the target mechanism. Of those springs which are expected to be heavily loaded a stress-analysis is made (Appendix I).

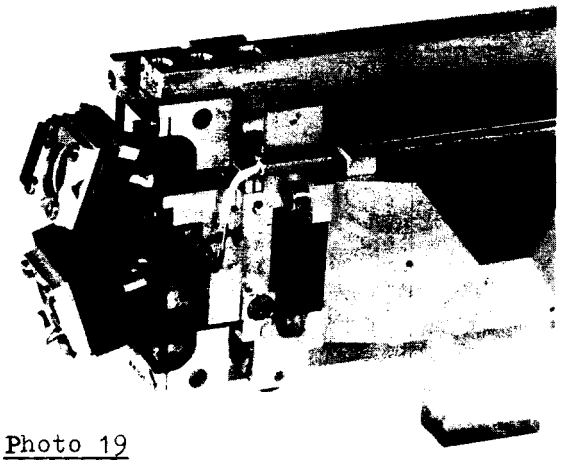

Photo 19

c) <u>The target arm and its fixation</u>

In order to be able to exchange targets easily without having to touch them (radio-activity levels of 40 rem/hr. have been measured) they are fixed to an arm of a certain length (photo 20).

Photo 20

This arm fits into the pivoting part of the target mechanism in a precisely reproducible way (Photo 21). At this point, an electrical contact is also made between the target, which is mounted insulated, and a shielded conductor, which leads to a coaxial plug on the outside

of the target chassis. The purpose of this is to measure the charge transported from the target by the charged secondary particles which escape from it under the influence of the traversing proton beam[9].

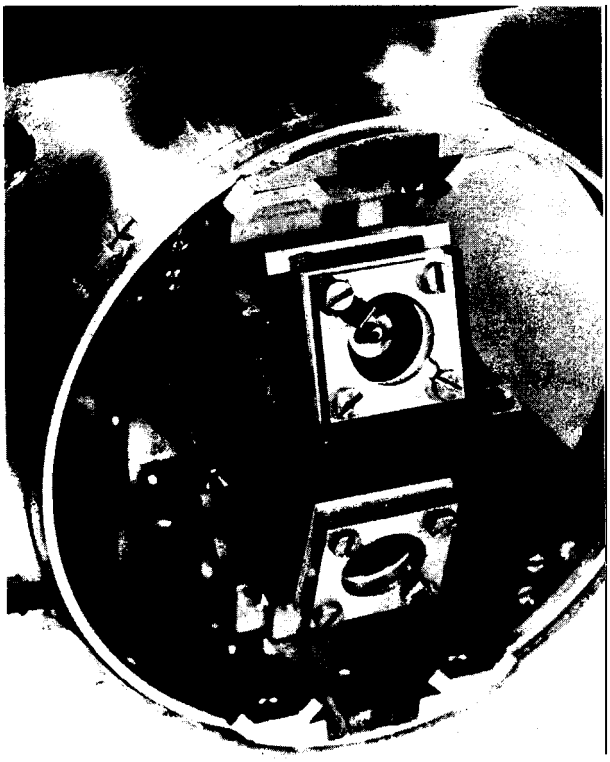

Photo 21

3. Operation

3.1 An example

To illustrate the possibilities of this mechanism and its small and stable rise and fall time, an oscillograph picture is shown below of an operation executed during week 49 in 1968. The experimenters using the beam from the target in ss 01 wanted, before their normal long burst at 26.4 GeV/c, a small burst (1% of the beam) at 14.5 GeV/c. Between the two, one or two bunches were ejected in the East Experimental Area.

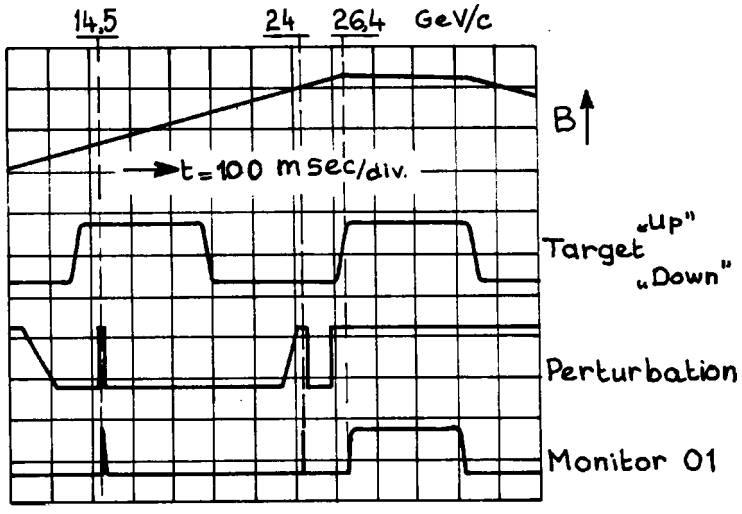

3.2 Alignment system

In order to be able to give the targets a precise position in the vacuum chamber, an alignment facility exists where the target, when fixed to the target unit, is projected doubly enlarged on a screen. There one can see if the target has the desired position and angle in the horizontal plane. At the same time, a telescope with a cross wire allows an observation in the vertical plane (Photo 22). On the righthand side of the picture one can see part of the control system, which is a complete double of the system in the MCR. With it we can check the proper functioning of all remote-controlled movements. It is also needed to put the target in its "up" position for the alignment procedure.

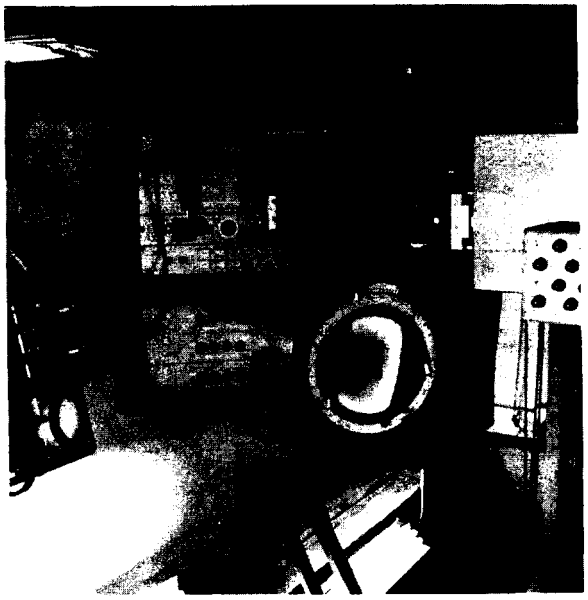

Photo 22

The target unit is positioned onto this device with a similar set of pins, as used in each standard target position in the ring. In each target unit, the position of the pivoting pieces which are the holders for the target arm, in relation to the positioning holes in the mounting flange, is adjusted to be the same for all units with a certain precision. This allows us to pre-align targets on their arms with the help of a jig which has only the arm-holder in its "up" position and the mounting flange with its location holes.

We can now exchange targets very rapidly without having to transport the unit to the hot lab. for alignment purposes.

3.3 Shielded vacuum storage

In order to have the target units close at hand in the hot lab., where they are prepared for operation and where maintenance is carried out, and without being continuously exposed to radiation from all of them, a shielded storage place was made. A big pit, 2.5 x 6 m^2 and 3 m deep is

covered by concrete blocks, 0.8 m high, resting on steps in the pit wall in such a way that their tops are at floor level. Photo 23 is a top view. Underneath these block trays and shelves are fitted and the equipment stocked there can be reached by using the lifting gear overhead. One block is larger than the rest and underneath is space for bigger parts such as external targets. One block carries on top a complete vacuum pump system. Up to seven target units can be kept at low pressure (Photo 24).

Photo 23

One can distinguish their black vacuum vessels and the valve with which they can be transported under vacuum into the ring to be installed with only a very short exposure to atmospheric pressure.

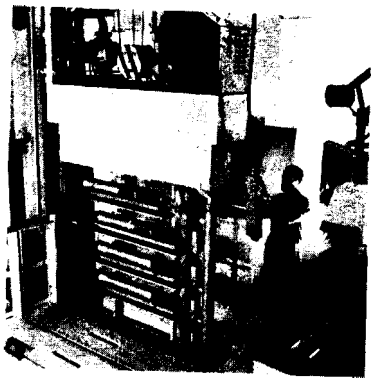

Photo 24

In another place, four small blocks take the space of one normal one. The trays underneath permit the storage of small parts. The bottom part is a container for radioactive waste (Photo 25).

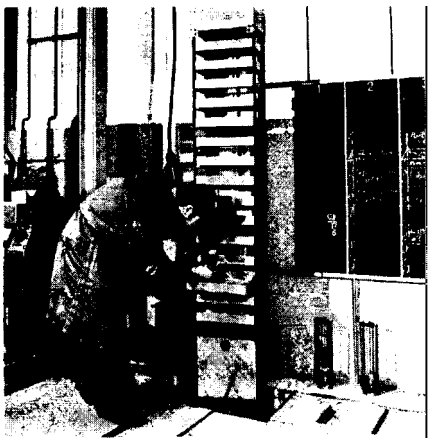

Photo 25

4. Conclusion

The system has now been in operation since October 1968, the end of the last shutdown. All targets for the physicists are normally moved with this mechanism.

Target mechanisms type '63 are still used extensively, mainly for machine development and beam measurements. The development of this new type has given us experience with servo mechanisms in such a way that future target developments can be expected to work also on this principle.

5. Acknowledgements

One can imagine that for the amount of work shortly described above, the close collaboration of an enormous number of people is required. We will therefore not attempt to list them for fear of forgetting somebody, but would like to make exceptions for Messrs. H. Bobillier, J. Comte, M. Corcelle and G. Willemin in the mechanical field, as well as for Messrs. J.P. Bovigny and Ch. Serre in the electronics field, whom we have to specially thank for their skillful assistance and their good ideas, and with whom it was a pleasure to work.

J.J. Merminod
M. van Rooy

/je

APPENDIX

The crossed strip hinges

Fig. 26 shows these springs in the two extrement conditions and Fig. 27 any one of the four springs A_1, B_1, A_2 and B_2.

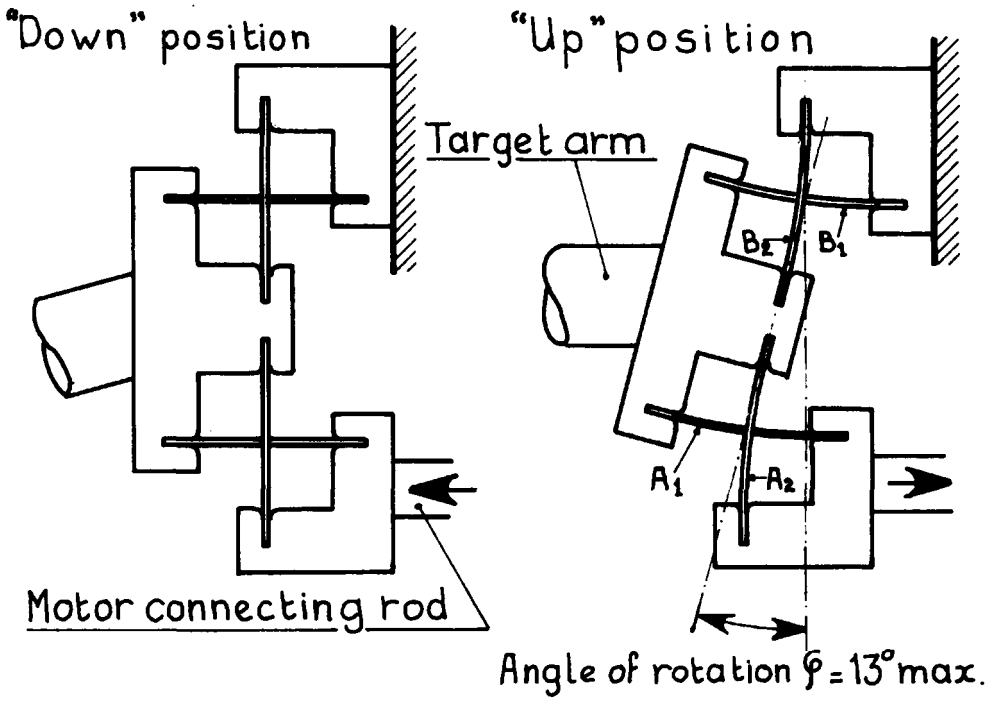

Fig.26 The crossed strip hinges

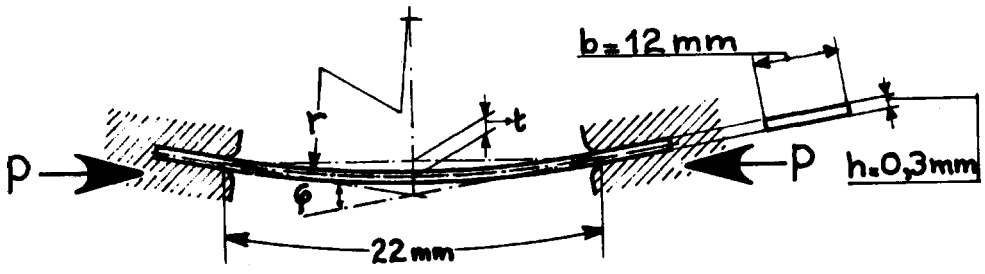

Fig.27 Shape of a single strip or spring

The force P depends upon the force the motor connection rod transmits. This force is represented in graph a), and it has to be transmitted by spring A_1. The angular speed ω of the target arm is represented in graph b) and the angle of rotation φ in graph c). The maximum of φ is 13° although for normal operation $\varphi_{max} = 11^\circ$. Of course the force in spring B_1 is exactly opposed to the force in spring A_1, since together they make the couple which rotates the target arm.

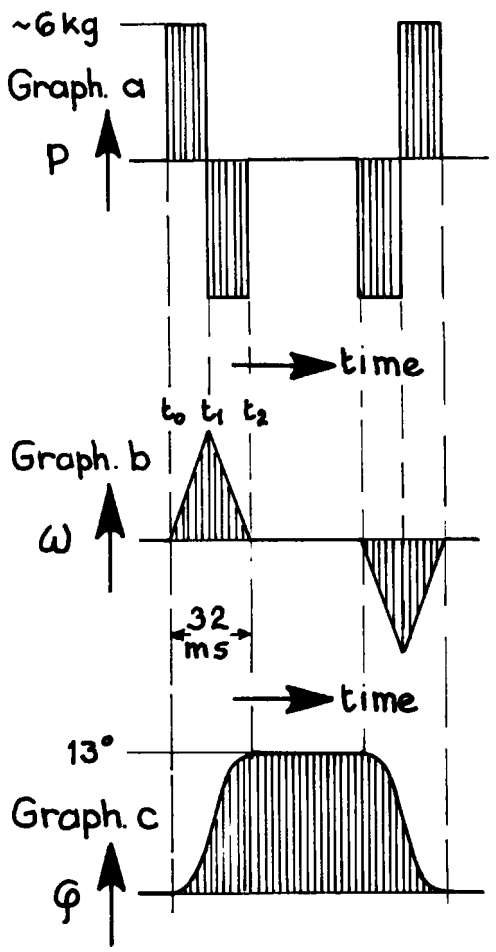

The forces in the springs A_2 and B_2 are much smaller and since they are of the same strength we will only analyse the springs A_1 and B_1 just before times t_1 and t_2.

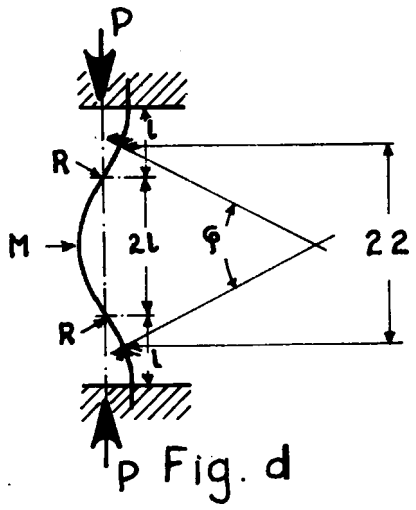

Fig. d

A_1 just before t_1

We will apply to these springs Timoshenko's theory of elastic stability[10] and also use his notations. The length 2ℓ of figure d), which represents the spring, may vary between 22 mm and half of this value but we will consider the most unfavourable case where $2\ell = 22$ mm. At the points R the curvature of the spring changes its sign and the line of action P passes through these points since the bending moments are zero there. This corresponds to the case of a loaded column (fig. e), built in at M of

the spring. In order to check if we can use Euler's formula to calculate P_{cr}, the load at which buckling starts, we have to calculate the slenderness ratio $\lambda = \frac{\ell}{k_z}$ where k_z is the ratio of gyration $\sqrt{\frac{I_z}{A}}$, for the smallest momentum of inertia I_z. A is the cross-sectional area.

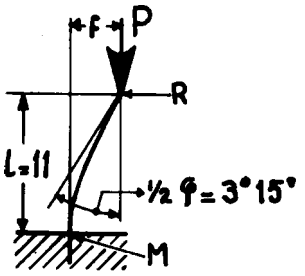

Fig. e

$$I_z = \frac{1}{12} bh^3 \text{ mm}^4 = \frac{1}{12} \cdot 12 \cdot 0.3^3 =$$

$$27 \cdot 10^{-3} \text{ mm}^4 \quad A = 12 \cdot 0.3 = 3.6 \text{ mm}^2$$

$$k_z = \sqrt{\frac{27.10^{-3}}{3.6}} \text{ mm} = 0.0865 \text{ mm.}$$

This gives a slenderness ratio $\lambda = \frac{\ell}{k_z} = \frac{11}{0.0865} = \sim 127$. The lowest value of λ for which Euler's formula can be applied to this material can be estimated at $\sqrt{\frac{\pi^2 E}{\sigma_{cr}}} \approx 45$ so we can indeed say

$$P_{cr} = \frac{\pi^2 E I_z}{4 \ell^2} = \frac{\pi^2 \cdot 11.10^3 \cdot 27.10^{-3}}{4 \cdot 11^2} \approx 6.05 \text{ kg.}$$

This means that for the pushing force in the motor connecting rod of 6 kg, the spring takes indeed the shape as indicated in fig. e) and the distance between the points R is 22 mm in fig. d).

In that case, we can calculate the biggest stress in this spring which occurs at M, by imagining the force P substituted by a force P', directed towards M and thus having almost no influence on the bending of the spring, and a force K, perpendicular to the spring. (f is of course highly exaggerated in the drawing). The force K creates the deflection f and gives to the end of the spring the angle $\frac{1}{2}\varphi = 3^\circ 15'$. From the mechanical handbooks[11] we learn that

$$\text{tg } \tfrac{1}{2}\varphi = \frac{3f}{2\ell} \rightarrow f = \frac{2\ell \text{ tg } \frac{1}{2}\varphi}{3} = \frac{2 \text{ x } 11 \text{ x } 0.057}{3} = 0.42$$

Applying this to fig. e), we find that P exerts on the spring in M a momentum of P x 0.42 kg mm which induces in the spring a bending stress $\sigma_b = \frac{M}{W_z}$ where $W_z = \frac{I_z}{\frac{1}{2}h} = 0.18$ mm ^{3}

$$\sigma_b = \frac{6 \times 0.42}{0.18} = 14 \text{ kg/mm}^2$$

which gives graph d) for the stresses in the spring, including a compression stress $\frac{P}{A} = 1.7$ kg/mm ^{2}.

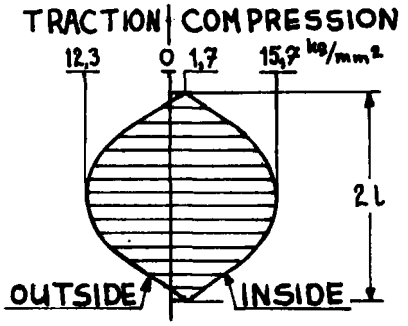

Graph. d

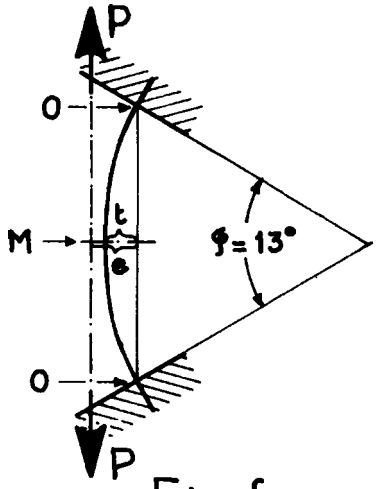

Fig. f

A_1 just before t_2

Instead of push, the spring has now to transmit a pulling force of ~ 6 kg, while being bent at an angle $\varphi = 13^\circ$. Since the bending radius at M does not need to be infinite, the line of action P passes there at a distance of e-t, giving thereby the necessary momentum P(e-t) to bend the spring at M (fig. f).

In fig. g), the loading case of this spring is represented with P acting directly at M. We imagine P split into two components, P' whose line of action passes through O and so has little influence on the bending of the spring and K, which is perpendicular to the spring at O.

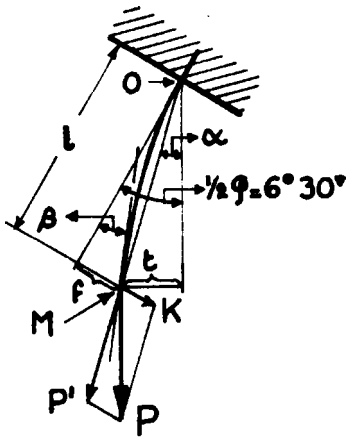

Fig. g

Here again, the angles φ, α and β as well as the distances f and t are highly exaggerated so we can say $K = P \operatorname{tg} \alpha$ which gives

$$f = 4\frac{\ell^3}{bh^3}\frac{K}{E} = 4\frac{\ell^3}{bh^3}\frac{P \operatorname{tg} \alpha}{E}$$

For the same reason $t + f = \ell \operatorname{tg} \frac{1}{2}\varphi$ and $t = \ell \operatorname{tg} \alpha \rightarrow f = \ell \operatorname{tg} \frac{1}{2}\varphi - \ell \operatorname{tg} \alpha$

$$\ell \operatorname{tg} \tfrac{1}{2}\varphi - \ell \operatorname{tg} \alpha = 4\frac{\ell^3}{bh^3}\frac{P \operatorname{tg} \alpha}{E} \rightarrow \operatorname{tg} \alpha = \frac{\ell \operatorname{tg} \frac{1}{2}\varphi}{\ell + 4\frac{\ell^3}{bh^3}\frac{P}{E}} = \frac{11 \times 0.114}{11 + 4\frac{11^3 \cdot 6}{12.0{,}3^3 \; 11.10^3}}$$

$$= \frac{1.26}{11 + 9} \approx 0.063 \rightarrow t = \ell \operatorname{tg} \alpha = 11 \times 0.063 = 0.7 \text{ mm.}$$

This gives the momentum of P on O with the bending stress $\frac{6 \times 0.7}{0.18} = 23 \text{ kg/mm}^2$.

The value of $f = \ell(\operatorname{tg} \frac{1}{2}\varphi - \operatorname{tg} \alpha) = \ell(0.114 - 0.063) = 0.561$ mm

$\rightarrow \operatorname{tg} \beta = \frac{3f}{2\ell} = \frac{1.683}{22} = 0.077.$

Of course $\operatorname{tg} \beta$ should be $\operatorname{tg} \frac{1}{2}\varphi$ since the spring does not show a sharp bend at M. From this we find the missing moment in fig. f) $P(e-t)$. Its value is found from the difference $\operatorname{tg} \frac{1}{2}\varphi - \operatorname{tg} \beta = 0.037 = \operatorname{tg} \gamma$. From the same handbooks[10] we learn $\operatorname{tg} \gamma = \frac{M\ell}{EI_z}$ where M is in this case the missing moment

$$\sigma = \frac{M}{W} = A = \frac{\operatorname{tg} \gamma \, EIz}{\ell \cdot W} = \frac{\operatorname{tg} \gamma \, E \, W.\frac{1}{2}h}{\ell \cdot W} = \frac{0.037 \cdot 11.10^3 \cdot 0.15}{11} = 5.5 \text{ kg/mm}^2$$

Graph e) gives the stresses in spring A_1 in this case, including a tensile stress of 1.7 kg/mm².

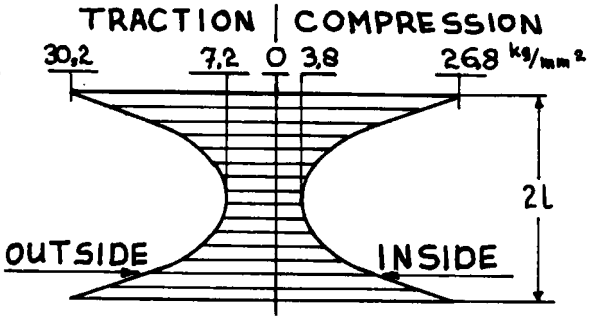

Graph. e

When we now bring together in one graph f) the stresses in this spring at the moments just before t_0, where they are zero, just before t_1, just before t_2 and after t_2,

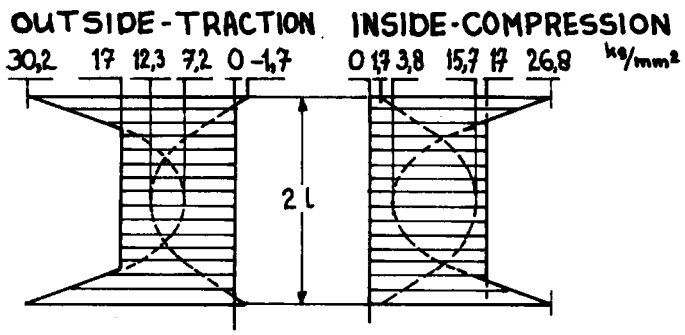

Graph. f

when there is a uniform bending stress all along the spring, of which the value can be found by substituting 0.114 for $tg\,\gamma$ in formula A, which gives $\sigma_b = 17$ kg/mm², then we can see the different stress variations which occur in this spring during one half duty cycle. It can be seen, without knowing the exact shape of the curves, that the maximum stress variation is 31.9 kg/mm² for spring A_1, occurring at the points where it is built in.

Spring B_1 just before t_1

We use fig. g) the only difference being the value of $\frac{1}{2}\varphi$ which is now $3^o\ 15'$

$$tg\,\alpha = \frac{\ell\ tg\,\frac{1}{2}\varphi}{\ell + 4\,\frac{\ell^3}{bh^3}\,\frac{P}{E}} = 0.0315 \qquad t = \ell\ tg\,\alpha = 0.34$$

Momentum on the spring at 0 = P x t .

Bending stress at 0 = $\sigma = \frac{P \times t}{W} = \frac{6 \times 0.34}{0.18} = 11.3$ kg/mm².

$f = \ell(tg\,\frac{1}{2}\varphi - tg\,\alpha) = 11(0.0570 - 0.0315) = 0.28.$

$tg\,\beta = \frac{3f}{2\ell} = 0.038$, this of course should be the value of $tg\,\frac{1}{2}\varphi = 0.057$. The tangent of the missing angle = 0.057 - 0.038 = 0.019 and the missing moment induces a bending stress of $\frac{0.019}{0.037} \times 5.5 = 2.8$ kg/mm². This, together with a pure tensile stress of 1.7 kg/mm², gives graph g) of the stresses in spring B_1 just before t_1.

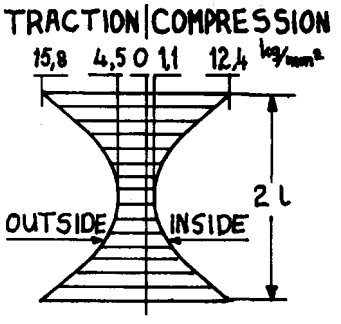

Graph. g

Spring B_1 just before t_2

This is almost the same situation as depicted in figure e), the only difference being the value of $\frac{1}{2}\varphi$ which is 6° 30' here. This gives for the deflection $f = \frac{2\,\ell.tg\,\frac{1}{2}\varphi}{3} = 0.835$, which corresponds not too badly with Timoshenko's table of load deflections[10] where with the interpolation $f = \frac{6.5}{20} \times 0.220 \times 11 = 0.79$ is found.

The value 0.835 gives a bending stress of $\frac{6 \times 0.835}{0.18} = 28\ kg/mm^2$. This combined with the pure compressive stress gives graph h) for this case.

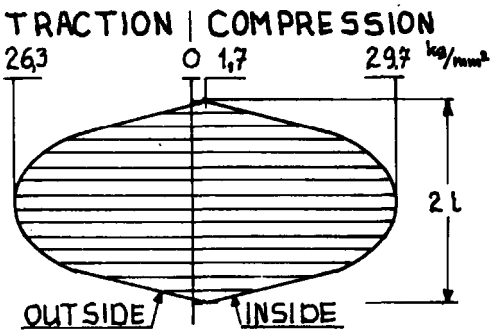

Graph. h

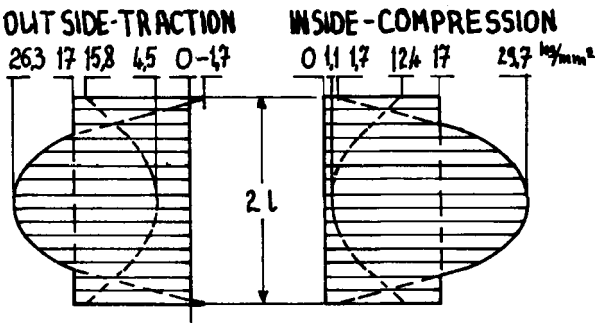

Graph. k

When we combine now agin for this spring the different stresses at the different moment as for spring A_1, then we have graph k), which shows us that the maximum stress variation for spring B_1 is 29.7 kg/mm^2, occurring in the middle.

In order to check something of these calculated figures, it was tried to measure these stresses. The bending stress in a bent spring is related to its bending radius "r" following the formula $\sigma_b = \frac{\frac{1}{2}h}{r} E$, where h is the thickness of the spring and E is the modulus of elasticity.

For the case considered, this means $\sigma_b = \frac{1650}{r}$. The bending radius needs to be measured along a small length of the spring since it varies along the length.

The method used is shown in figure 1) and consists of observing via a telescope with cross-wires two lighted slits which have a known distance

t, using the chromed surface of the bent spring as a mirror. For small values of α one can say $\alpha = \frac{p}{r}$ and $2\alpha = \frac{t-p}{\ell} \rightarrow r = \frac{2p\ell}{t-p}$ where p is the vertical displacement of the telescope, necessary to move the cross-wires from being centered on the image of one slit to being centered on the other.

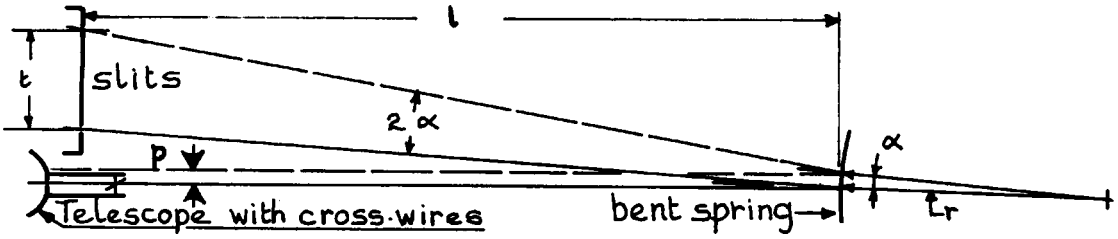

Fig. l

Result

For the situation depicted in graph f), where the stress variation due to bending is calculated to be 28.5 kg/mm², the measured value is 27 kg/mm².

For the situation shown in graph k), which is calculated to give a stress variation due to bending of 28 kg/mm², the measurement showed a figure of 25 kg/mm².

For the first case, one has to add 3.4 kg/mm² to get the total stress variation and for the second 1.7 kg/mm².

The figures found in reference 12 give maximum stress variations between 30 kg/mm² and 31 kg/mm². This means that these springs are working fairly close to their maximum possibilities, although one should take into account that

a) the force of 6 kgs is measured under static conditions; under dynamic conditions the force necessary to accelerate the motor connecting rod and all the parts fixed to it does not have to be transmitted by this spring.

The acceleration of these parts is $\frac{2s}{t^2} = \frac{2 \times 3 \times 10^{-3}(mm)}{16^2\ 10^{-6}(sec)} =$ 23 m/sec². The weight of these parts is about 0.4 kg, so they take from this force $0.4 \times \frac{23}{10}$ kg $\approx$ 0.9 kg to accelerated themselves and the spring has to transmit the rest which is $\sim$ 5.1 kg under normal working conditions.

b) The angle of rotation φ used to calculate the stress is 13° but normally φ wil never exceed 12°, which corresponds to a vertical position of 3 mm across the middle of the chamber.

Practice has proved that with careful mounting these springs will hold.

REFERENCES

1) H. Fisher and W. Richter, Production of secondary beams at the CERN Proton Synchrotron, Proceedings of the 1961 International Conference on High-Energy Accelerators

2) E. Brouzet, Mesures des dimensions transversales du faisceau interne PS à moyenne et haute énergie, MPS/Int.CO 68-21

3) C. Bovet and D. Dekkers, Proton utilization at the CERN Proton Synchrotron, MPS/Int.CO 67-14

4) J.H.B. Madsen, Radiation dose measurements around the PS vacuum chamber, MPS/Int.CO 66-4

5) G. Pluym and M. Van de Voorde, Radiation damage tests on epoxy resins, ISR-Mag 67-3

6) K.H. Reich, Information for physicists concerning the PS targets, PS/Int. MG/VA 60-15

Th. Sluyters, PS internal targets as a nuclear physics tool, MPS/Int VAC 61-17

W. Richter and M. van Rooy, Internal targets for the CERN PS ('63) MPS/Int.CO 66-18

7) P.H. Standley, The CPS Improvement Programme, MPS/Int.DL 65-12

8) J.P. Bovigny, L'appareillage de commande des cibles internes type '63, MPS/Int.CO 64-11

9) K. Budal, Charge transport from targets in proton beams, as a means of monitoring, CERN 67-17

10) Timoshenko and Gere, Theory of elastic stability, McGraw Hill Book Company Inc.

11) Dubbel, Taschenbuch für den Maschinenbau Springer Verlag

12) Ronald D. Crooks and William R. Johnson, Mechanical properties of beryllium copper wire and springs, Metal Progress, May '64

* * *